Hydrogenation/hydrodeoxygentation selectivity modulation by co-metal addition to palladium on carbon-coated supports

Alireza Saraeian[a,b], Geet Gupta[a], Robert Johnson[b,c], Rick W. Dorn[d,e], Hamed Bateni[a], Jean-Philippe Tessonnier[a,b], Luke T Roling[a], Aaron J. Rossini[d,e], Brent H. Shanks*[a,b]

[a] Department of Chemical and Biological Engineering, Iowa State University, Ames, IA, 50011, United States

[b] Center for Biorenewable Chemicals (CBiRC), Ames, IA 50011, United States

[c] Hawaii Natural Energy Institute, University of Hawaii at Manoa, Honolulu, Hawaii 96822, United States

[d] US Department of Energy, Ames Laboratory, Ames, Iowa 50011, United States

[e] Department of Chemistry, Iowa State University, Ames, Iowa 50011, United States

*: E-mail: bshanks@iastate.edu; Fax: 01 515 294 2689; Tel: 01 515 294 1895

Abstract

A series of carbon-supported palladium catalysts was synthesized to study the influence of binary Pd-metal catalysts on the selectivity of condensed phase hydrogenation reactions. Conversion of acetophenone and 1-phenylethanol using a lab-scale plug flow reactor was used to assess how the different bimetallic systems altered reaction selectivity between hydrogenation of either the aromatic ring or carbonyl group versus hydrodeoxygenation. A variety of co-metals including alkali and alkaline earth metals and transition metals were screened in this study. These results showed that the Pd-metal bimetallic catalysts led to dramatic shifts in selectivity compared to the Pd monometallic catalysts. Most notably, with the addition of iron, ethylbenzene was exclusively produced as the final product, while the addition of lithium yielded more than 80% phenyl hydrogenation products with little deoxygenation. To investigate how co-metal addition alters electronic states of Pd active sites various characterization techniques were employed to compare differences in acidity, oxidation states, oxygen affinity, and electronic properties. The experimental results and DFT calculations suggest the incorporation of lithium into the Pd lattice leads to the blockage of interstitial Pd-H formation through a higher formation energy compared to surface Pd-H and inhibits deoxygenation, whereas the addition of iron leads to the formation of a phase with higher affinity toward oxygen, thereby increasing the selectivity to deoxygenation. The findings of this work provide a model system to study the influence of bimetallic catalysts on reaction selectivity on carbon supports without introducing complicating factors such as pore size and heteroatoms that are difficult to control with traditional carbons used in commercial processes, and serves to provide insights that could be applied to additional processes such as selective hydrogenation of bio-derived chemicals.

Keywords: *Pd bimetallics; Carbon-supported catalysts; Selective Hydrogenation; Hydrodeoxygenation; Selectivity modulation*

Introduction

Development of heterogeneous catalysts to selectively hydro(deoxy)genate specific functional groups for reactions in the condensed phase will be critical for production of commodity and specialty chemicals from biomass-derived molecules. Condensed phase hydrogenation and hydrodeoxygenation reactions are critical for various processes including bio-fuels,[1-2] biochemicals,[3-4] pharmaceuticals,[5-7] and petrochemicals,[8-10] with heterogeneous catalysts desired due to their economic advantages. Controlling such reactions could result in selective product diversification from biomass-derived mixtures such as bio-oils, which would create new opportunities to improve the economics of biorefineries, especially in the context of bioprivileged molecules.[11] Therefore, even if modulating the selectivity toward a specific reaction and particular products is not urgent at this point, it is absolutely necessary for preparing a catalytic "toolbox" for selective production of high-value chemicals from highly-functionalized molecules derived from biomass.

Development of highly selective heterogeneous catalysts that can be sensibly manufactured at commercial scales and are resistant to deactivation is a significant technical challenge. From the perspective of maximizing selectivity, approaches to tether organometalics onto silica or alumina supports is often investigated.[12-16] However, these catalysts are expensive to produce and very often suffer from deactivation when on stream for an extended period of time, resulting from leaching of active sites and molecular decomposition.[3, 14, 17-19] Alternatively, supported metal nanoparticles (NPs) are more commercially viable to produce and are stable for longer periods on stream, but it is challenging to synthesize catalysts that provide control over product selectivity.[3, 12 20-21] Extensive research has been devoted to understanding how to modulate metal NP active sites to improve catalyst properties through alteration of various factors including particle size and shape,[22-23] metal-support interactions,[24] and metal alloying effects.[20, 25] In particular, formation of metal NP alloys can result in alterations to catalytic properties by modifying the metal electronic properties,[26-27] metallic geometry,[27-28] lattice spacing, and site morphology.[20] It has been shown that models predicting alloying electronic effects in heterogeneous catalysis can be established and used to expedite catalyst design.[29-30]

An additional consideration for condensed phase heterogeneous catalysts is the stability of the support material to resist fouling and chemical breakdown. Metal oxides such as zeolites, mesoporous silica, and alumina have been shown to be significantly less stable as support materials compared to carbon supports, which can withstand harsh hydrothermal conditions and at elevated temperatures, and resist fouling due to their hydrophobicity.[14, 18, 31-32] For these reasons, carbon-supported catalysts are most likely required for further expansion of bio-based chemical processes and biorefineries.[3, 32]

Systematically studying carbon-supported catalysts, however, poses unique challenges that require significant effort to overcome. This issue is partially because commercially available carbon supports (e.g., carbon black, charcoal, and activated carbon fibers) have large pore size distributions, containing a significant fraction of micropores that contain impurities from the precursor materials, and require polymeric binders to produce pellets needed for use in flow reactors. These factors introduce additional variability and

experimental challenges that are difficult to control. To address these issues, the current work used a synthesis procedure that produced templated mesoporous carbon supports with controlled pore structure.[31, 33]

Bimetallic nanoparticle catalysts are a potential solution for the selective hydrogenation and hydrogenolysis of bio-based molecules.[34] Additionally, mesoporous carbon-metal oxide supports can be synthesized and PdFe bimetallic NPs can be immobilized on these supports.[26] The formation of these bimetallic phases were supported by experimental evidence showing differences in CO chemisorption, H_2-TPD profiles, and lattice d-spacing as measured by high resolution TEM. Similarly, electron transfer from Fe to Pd was found to be responsible for the high yield of aromatics obtained from selective cleavage of benzyl phenyl ether.[35] This effect was also manifested as small shifts in the XRD and XPS spectra as well as significant changes in H_2-TPR and H_2-TPD profiles. Testing showed that PdFe alloy catalysts had a higher activity for hydrogenation of C=O bonds than a single metallic Pd catalyst, demonstrated by higher apparent turnover frequency of acetone hydrogenation to isopropanol under conditions similar to the current work.[26]

Herein, the previous work is expanded by incorporating various metal species to investigate the role of co-metals on the selectivity of Pd catalysts for hydrogenating ketone C=O bonds versus aromatic C=C bonds, and hydrogenolysis of C-O bonds under condensed-phase conditions. Acetophenone (AP) and 1-phenylethanol (PE) were chosen as the primary model compounds for this reaction system to study the network consisting of multiple hydrogenation and hydrodeoxygenation reactions occurring in both series and parallel. An overview of the reaction network over Pd catalysts is shown in **Scheme 1**.

Previously, mechanistic studies of AP hydrogenation revealed that the nature of the reactant's interaction with the catalyst surface leads to substantial changes in the product selectivity,[36] particularly relating to the role of the respective carbonyl group and aromatic ring adsorptions. Related studies for furfural and guaiacol conversion on bimetallic PdFe showed weakening of ring adsorption disfavored ring hydrogenation and favored C=O hydrogenation.[37-38] McEwen and coworkers observed the adsorption strength of the aromatic ring decreased on PdFe in comparison with pure Pd observed shifts in the Pd *d*-band center in the presence of Fe.[39-40] Based on these studies, it was proposed that surface bound hydrogen is primarily responsible for the hydrogenation of the aromatic ring and carbonyl group. However, subsurface hydrogen has also been reported by Ashwell et al. to play a role in altering hydrodeoxygenation energetics of the carbonyl moiety.[41] Interestingly, light metals such as lithium or boron can occupy interstitial sites in the Pd lattice denying access of hydrogen to the subsurface, and thereby restricting the hydrodeoxygenation of the carbonyl moiety in aromatic ketones.[42-43]

Experimentally, the product distribution obtained when various carbon supported Pd-metal bimetallics were used as catalysts for the hydrogenation of acetophenone (AP) and 1-phenylethanol (PE) in order to obtain a characterization of the overarching selectivity effects caused by addition of different metals to the bimetallics. Density functional theory (DFT) calculations were used to elucidate fundamental ‘ensemble and electronic effects’ governing the hydrogenation selectivity.

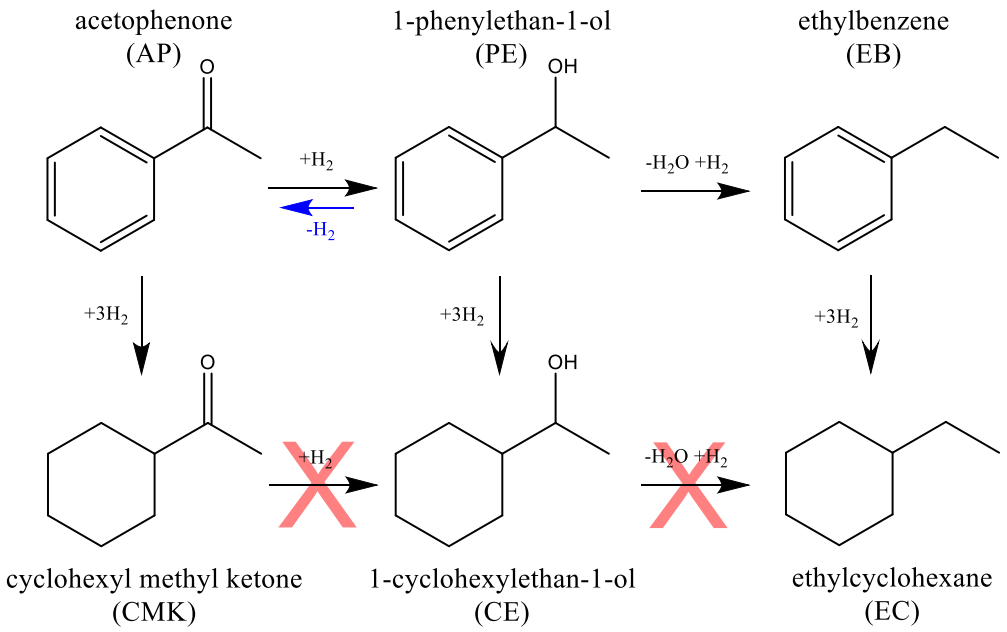

Scheme 1. Reaction network of acetophenone over Pd catalysts at 200 °C and 5 MPa H_2 (red x's mark the reaction pathways that were found not to occur).

Experimental Section

Materials and catalyst synthesis

Acetophenone (Alfa Aesar, 99%), 1-phenylethanol (Sigma-Aldrich, 98%), ethylbenzene (Alfa Aesar, 99%), cyclohexyl methyl ketone (Alfa Aesar, 95%), 1-cyclohexylethanol (Alfa Aesar, 98%), and ethylcyclohexane (ACROS Organics, 99+%) were used in the reaction studies or calibration standards without further purification. Ethanol (200 proof) was used as the solvent for preparing both the reactant feed and the standard solutions.

A detailed description of the catalyst synthesis procedure is included in the Supporting Information (SI) and **Figure S1**. Briefly, the porous silica support was impregnated with a co-metal, carbon from furfuryl alcohol, and Pd, in that order, yielding different bimetallic catalysts. Co-metal selection was initially guided by differing oxophilicity as reported by Keep et al.[44] Impregnation with furfuryl alcohol to form a thin layer of carbon on top of the silica support was adopted from Joo et al.[5] The presence of the carbon coating limited the final catalyst annealing temperature to 300 °C. This synthesis method allowed for an easier transfer of the catalyst into the reaction beds as it formed of pellets rather than powder due to reduced static repulsion.

Catalyst characterization

A list of characterization techniques and their purposes are briefly mentioned below. These techniques are described in more detail in the Supporting Information.

- Inductively coupled plasma-optical emission spectrometer (ICP-EOS) was used to determine metal loadings.
- N_2-physisorption analysis was used to determine the surface area and pore size distribution of the catalysts.
- X-ray photoelectron spectroscopy (XPS) was used to examine on the Pd oxidation state.
- Both CO and H_2 chemisorption were performed to estimate Pd dispersion and average particle size.
- XRD and TEM were performed to examine alloying and particle size.
- Ammonia temperature-programmed desorption (NH_3-TPD) measure the acidity of the catalysts, whereas hydrogen temperature-programmed desorption (H_2-TPD) was used to reveal the relative bonding strength of hydrogen on the Pd NPs.
- Thin-film solid-state nuclear magnetic resonance (NMR) spectroscopy was performed to provide additional information about the interaction of oxygenated molecules with the catalyst surface.

Catalytic performance measurements

The reactions were performed in a continuous up-flow stainless steel reactor with an ID of 6 mm. In a typical experiment, 10 mg of catalyst was packed between two layers of glass wool (Sigma-Aldrich, Silanized) sandwiched by silicon dioxide chips (Sigma-Aldrich, 4-20 mesh, 99.9% trace metal basis). The reactor typically operated at 200 °C and 5 MPa of pressure with a H_2 flow rate of 100 ml/min. The catalysts were reduced overnight at 200 °C and 5 MPa under 50 ml/min H_2. The reactor temperature was controlled using a benchtop controller (Omega, CSi32K) with a K-type thermocouple used to measure the temperature as close as possible to the catalyst bed. High-wattage heating tape over a cylindrical aluminum block surrounding the stainless-steel tubing was used to heat the reactor. The reactor pressure was controlled using a back-pressure regulator and monitored using two pressure gauges downstream and upstream. An HPLC pump was used to inject the feed with a typical flow rate of 0.2 ml/min. Samples were collected every 1 h for at least 8 h and the results reported were average values from samples 2-8, unless stated otherwise.

Product analysis

Product analysis was done using a gas chromatograph (GC – Agilent 7890A) equipped with a mass spectrometer (MS – Agilent 5975C) for identification and a flame ionization detector (FID) for quantification of the compounds. The FID was calibrated using a 5-point calibration curve. The GC oven was programmed to initiate at 50 °C, hold for 5 min, and then ramp to 200 °C at 10 °C/min. A highly polar column (Agilent DB-WAX) was used to separate the products.

The conversion of reactant, and yield and selectivity of products are reported on a carbon basis using the following equations:

$$Conversion\ (C\%) = \frac{carbon\ mass\ of\ consumed\ reactant}{carbon\ mass\ in\ reactant\ feed} \times 100\% \quad (1)$$

$$Yield\ (C\%) = \frac{carbon\ mass\ of\ product}{carbon\ mass\ in\ reactant\ feed} \times 100\% \quad (2)$$

$$Selectivity\ (C\%) = \frac{carbon\ mass\ of\ product}{carbon\ mass\ of\ all\ products} \times 100\% \quad (3)$$

Computational Methods

DFT calculations were performed using the Vienna ab initio simulation package (VASP), a periodic, plane wave-based code.[45-46] Projector augmented wave potentials (PAW-PBE) were used to describe the electron-ion interactions;[47] van der Waals corrections were implemented through the optB88-vdW functional as proposed by Klimeš[48-49] as dispersion effects have been shown to be significant in the adsorption of aromatic rings.[50] The plane-wave basis set was expanded with a kinetic energy cutoff of 400 eV and with an electronic energy precision and maximum force tolerance of 10^{-4} eV and 0.05 eV/Å, respectively, for geometry optimizations. The DFT-optimized lattice constants in Å (experimental values in parentheses) were 3.935 (3.890)[51] for *fcc* Pd and 3.882 (3.852)[52] for bimetallic *fcc* Pd_3Fe.

Geometry optimizations were performed for all surfaces using a (4x4) surface unit cell with four total atomic layers and the bottommost two-layers fixed at their bulk-optimized coordinates, except as noted below for the model with subsurface Li. All other atoms in the other modeled surfaces, including adsorbates, were allowed to fully relax. All surface unit cells contained a vacuum layer between successive slabs equivalent to six atomic layers. The surface Brillouin zones were sampled with a 2x2x1 k-point grid based on the Monkhorst-Pack scheme.[53] Gas phase calculations were performed in a large supercell (20 Å x 21 Å x 22 Å) using only the gamma point.

All gas phase Gibbs free energies (G) were calculated in the following manner:

$$G = E + ZPE - TS \quad (4)$$

where E is the total energy of the gas phase species, ZPE is the calculated zero-point energy correction of the gas-phase species, T is the absolute temperature, and S is the calculated entropy of the gas-phase species. ZPE and S were estimated from vibrational frequency calculations, including translational, vibrational, and rotational modes, which were calculated by numerical differentiation of forces using second-order finite differences with a step size of 0.015 Å.

Free energies of adsorbed species (G_{ads}) were calculated relative to the free energies of gas-phase acetophenone, H_2, and H_2O, and the total energy of the clean slab (E_{slab}) as follows:

$$G_{ads} = (E_{ads} + ZPE_{ads} - TS_{ads}) - E_{slab} - G_{AP,g} - \frac{m}{2} * G_{H_2,g} + n * G_{H_2O,g} \quad (5)$$

where E_{ads} is the total energy of the adsorbate on the slab, ZPE_{ads} and S_{ads} are the zero-point energy and entropy of the adsorbed species calculated on Pd(111) and utilized for all the modeled surfaces, and m and n are coefficients for stoichiometric balance. . $G_{AP,g}$, $G_{H_2,g}$, and $G_{H_2O,g}$ are the gas phase free energies of acetophenone (AP), hydrogen, and water, respectively. All free energies are calculated at 200 °C and 5 MPa pressure to match the experimental reaction conditions. Additional details about bimetallic model construction can be found in the SI.

Results and Discussion

Initial screening of the reaction network

Hydrogenation of the C=O bond in acetophenone (AP) to form 1-phenyl ethanol (PE) has been reported over Pd/C and Pd/Al_2O_3 catalysts at temperatures as low as 15 °C with slow kinetics for deoxygenation to ethylbenzene (EB) and almost no phenyl hydrogenation.[54-56] In another example, Pd/SiO_2-Al_2O_3 catalyzed C=O hydrogenation at a low temperature and H_2 pressure (15 °C and 0.3 MPa)[56] with only minor cyclohexyl methyl ketone (CMK), ethylcyclohexane (EC), or cyclohexyl ethanol (CE) at 60 °C,[57] whereas at a higher temperature of 170 °C and 5 MPa, H_2 formed measurable amounts of these products, though individual selectivities were not reported.[58] In another work, aromatic ring hydrogenation did not happen even at 130 °C using either Pd/C or Pd/Al_2O_3 as catalysts.[59]

In agreement with these reports, AP hydrogenation over the monometallic Pd catalyst (i.e., 1PdC as described in the SI) at 160 °C showed minimal phenyl hydrogenation of AP and PE as compared to deoxygenation to EB and phenyl hydrogenation of EB to EC, initially suggesting C=O hydrogenation was more favorable than phenyl hydrogenation over this catalyst (**Figure 1**). At 240 °C, the selectivity of AP hydrogenation to CE, CMK, EB and EC products were distributed evenly; however, C-C coupling by-products were also observed, which lowered the overall carbon balance and could increase the rate of catalyst deactivation. Therefore, 200 °C was chosen as the operating temperature since good carbon balances (~100±5%) and reasonable selectivity distributions were obtained.

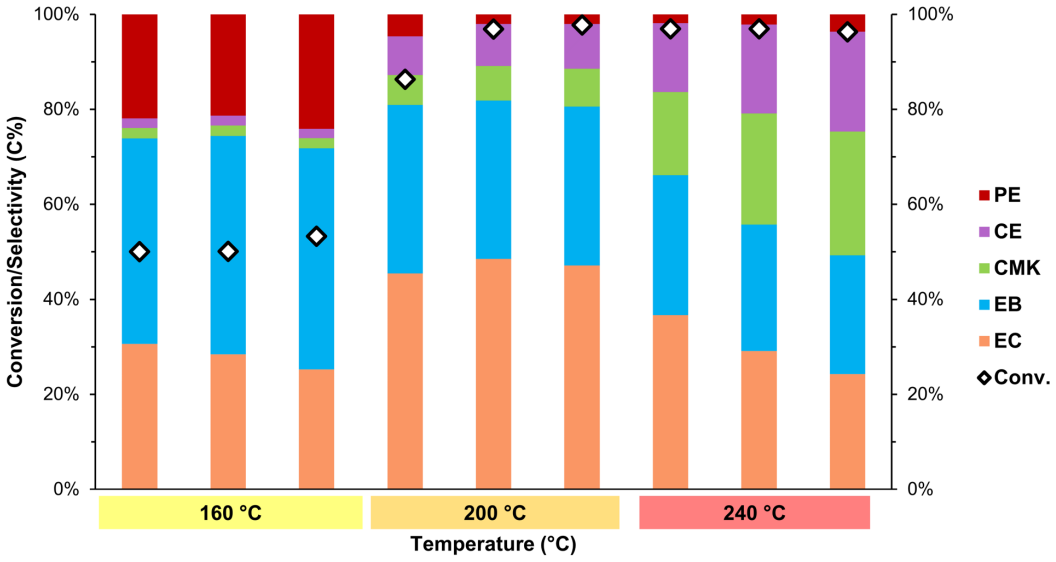

Figure 1. Acetophenone conversion over 1PdC at T=160-240 °C (20 mg catalyst, 100 ml/min H_2, 0.2 ml/min feed rate, 0.1 M AP/ethanol, P = 5 MPa)

Screening experiments were done for conversion of PE to determine the effect of co-metals on product selectivity. A range of co-metals were examined with their oxophilicity, electronegativity and ability to alloy

with Pd at 200 °C given in **Table S1**. The results showed that the co-metal addition could dramatically altered the selectivity observed for PE conversion (**Figure 2**). , The incorporation of Li as the co-metal diminished conversion while selectively blocking PE deoxygenation primarily leading to the formation of CMK and CE. Whereas, the addition of either Fe or Ga maintained PE conversion while promoted C-O scission and essentially eliminating phenyl hydrogenation.

Bimetallic PdFe was previously identified to have higher C=O hydrogenation activity than monometallic Pd in the conversion of acetone to isopropanol.[26] In this study, PdFe was found to achieve similar PE conversions compared to the Pd catalyst, while considerably higher selectivity to EB and almost no phenyl hydrogenation was observed, which suggested enhanced interaction of the oxygen atom with the PdFe particles. DFT calculations on a model PdFe surface was consistent with this hypothesis that PdFe particles strongly interacted with the oxygen atoms of AP (see discussion below).

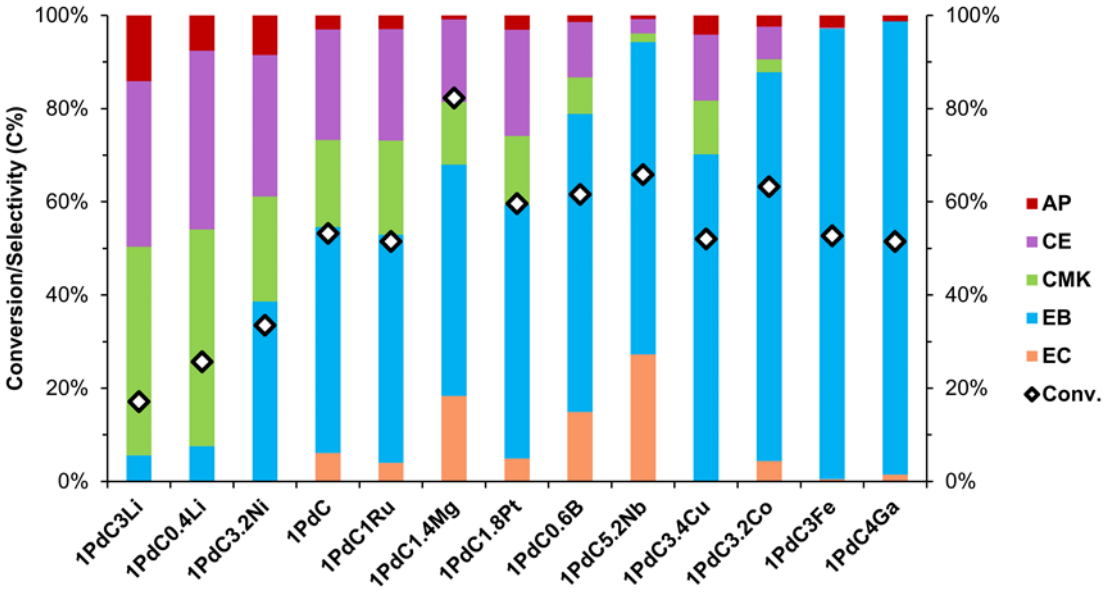

Figure 2. Catalyst screening for conversion of PE over Pd-M catalysts (10 mg catalyst, 100 ml/min H2, 0.2 ml/min feeding rate, 0.2 M PE/ethanol, T = 200 °C, P = 5 MPa).

Given their significant difference in selectivity, incorporation of Fe or Li were used for comparison with monometallic Pd in further studies. To investigate the AP catalytic reaction pathway including phenyl (C=C) versus carbonyl (C=O) hydrogenation and C-OH cleavage, experiments were conducted using AP, PE, EB, CMK, and CE feeds over Pd, PdFe, and PdLi catalysts. It has been previously proposed that EB is produced from AP via hydrogenation of C=O bonds to C-OH followed by dehydration-hydrogenation of C-OH with minimal C=O hydrogenolysis over supported Pd catalysts.[59] In addition to the expected formation of hydrodeoxygenation and hydrogenation products (i.e., EB, CE, and EC), AP and CMK were also produced from PE indicating the occurrence of C-OH dehydrogenation and phenyl ring hydrogenation under the

reactions conditions (**Table S2**). No conversion was observed for CE and CMK over any of the catalysts at 200 °C and 5 MPa H_2, suggesting that CE and CMK were both formed directly via phenyl hydrogenation and were not intermediate products during AP hydrogenation (**Scheme 1**). This result was in contrast with reports proposing the hydrogenation of CMK to CE and hydrogenolysis to EC as a potential pathway over Pd catalysts.[60-61] However, EB hydrogenation to EC occurred over all three catalysts, with 1PdC having the highest conversion at 10.6%, 1PdC0.4Li at 7.2%, and 1PdC3Fe with the lowest conversion at 2.6% (**Table S2**), which confirmed the impact of Fe addition in limiting aromatic ring hydrogenation even in the absence of oxygen moieties. Expectedly, no cyclohexane dehydrogenation was observed for CMK, CE, and EC. Based on these results, **Scheme 1** appeared to be an accurate representation of the reaction network under the conditions used in this study.

Catalyst characterization

Table 1 presents the metal loadings, Pd particle size, and textural properties for the catalysts. The co-metal addition led to a decrease in pore volume relative to the Pd-only catalyst. The average size of the Pd NPs calculated from CO chemisorption measurements seemed to vary slightly across the catalyst samples. The size dependent electronic and catalytic properties of Pd clusters arises primarily because the ratio of surface versus bulk H atoms will vary, as has been previously established;[62-63] however, significant differences in such properties were generally observed for extremely small sizes: from atomic scale to ~6 nm.[64] Larger particles would act similar to bulk Pd as reported previously from CO adsorption energies.[65] While the differences in average Pd particle size and potential variations in particle size distribution could influence reaction selectivity, it is unlikely that these differences in the range of ~6-10 nm can account for the significant differences in product distribution when using either monometallic or bimetallic materials. The relative similarities in macroscopic properties of the Pd, PdFe and PdLi catalysts suggest that the large differences in product distribution should mostly be explained by other factors such as the local electronic structure of the active sites, adsorption energies, and/or steric hinderance effects.

Table 1. Summary of catalyst characterization results

Sample	Pd [a] wt%	Fe [a] wt%	Li [a] wt%	S_{BET} m^2/g	Pore volume [b] cm^3/g	Pore size [c] nm	Particle size [d] nm
C/Davisil	-	-	-	264.2	0.603	9.9	-
1PdC	0.7	0	0	248.8	0.587	9.7	9.4
1PdC3Fe	0.8	2.1	0	282.6	0.461	7.6	7.4
1PdC3Li	0.9	0	2.1	-	-	-	-
1PdC0.4Li	0.9	0	0.2	165.0	0.462	8.7	6.1

[a]: Measured using ICP-EOS, [b]: Single point adsorption total pore volume of pores less than 253.5 nm diameter at ~p/p^0=0.99, [c]: Average pore diameter calculated from the desorption branch of the BJH method, [d]: Active particle diameter calculated from CO chemisorption data assuming hemispherical particles and a stoichiometric ratio of 1.

Representative TEM images for the catalysts are given in Figure S2. The average particle sizes determined from the images were 3.4, 5.5, and, 2.7 nm for 1PdC, 1PdC3Fe, and 1PdC0.4Li, respectively. The low concentration of the palladium (<1%) and the placement of the particles inside the mesoporous carbon support created a substantial challenge in rigorous evaluation of the particle sizes from the images. The lower values seen from TEM relative to those determined from chemisorption analysis could be due to the particles being embedded within the carbon coating and selective blocking of sites in the case of Li incorporation. In the case of 1PdC3Fe, larger aggregates of Fe were observed along with smaller particles of Pd leading to a larger average particle size value. EDS analysis suggested the presence of some sub-nanometer clusters of Fe and Pd dispersed on the support, which fell below or at the TEM resolution threshold. Unfortunately, the detection limitations of the instrument did not allow for precise deteremination of the Pd-Fe arrangement within the nanoclusters. Additionally, XRD analysis did not provide definitive demonstration of the crystalline state of the particles likely to the low loading and small particle sizes.

The NH_3-TPD results as shown in **Figure 3a** demonstrated a small quantity of acid sites on 1PdC while the acid sites were even lower in catalysts with co-metals. Total acidities were 281, 154, 162 μmol NH_3/g for the Pd, PdFe, and PdLi catalysts, respectively (**Figure S3**). While hydrodeoxygenation over heterogeneous catalysts is generally believed to require both metallic and acidic sites,[66-68] the reduction in acidity of PdFe compared to the monometallic Pd catalyst simultaneously with a higher deoxygenation selectivity over PdFe suggested limited contribution from the dehydration/hydrogenation pathway for deoxygenation of PE to EB. Additionally, PE did not react over the carbon support (i.e., C/Davisil) or over Fe or Li catalyst samples (without Pd); thus, PE dehydration due to support/co-metal acidity was ruled out as being important.

Figure 3b shows the H_2-TPD profiles for the Pd, PeFe, and PdLi catalysts. In these experiments, the reduction of the Pd catalysts was performed under flowing hydrogen at 0.1 MPa, which would likely result in the formation of Pd hydride phases. It is generally accepted that hydrogen stored inside the Pd lattice (in the interstitial sites) desorbs at or above 300 °C.[69] Thus, the peak at ~430 °C likely indicated the presence of Pd hydrides (Pd-H), with the concentration of Pd-H species decreasing somewhat for PdFe and

decreasing significantly for PdLi (**Figure 3b**). The much lower concentration of Pd-H for PdLi could be due to the penetration of Li into the Pd lattice, filling the interstitial sites and denying access to hydrogen as postulated previously.[70]

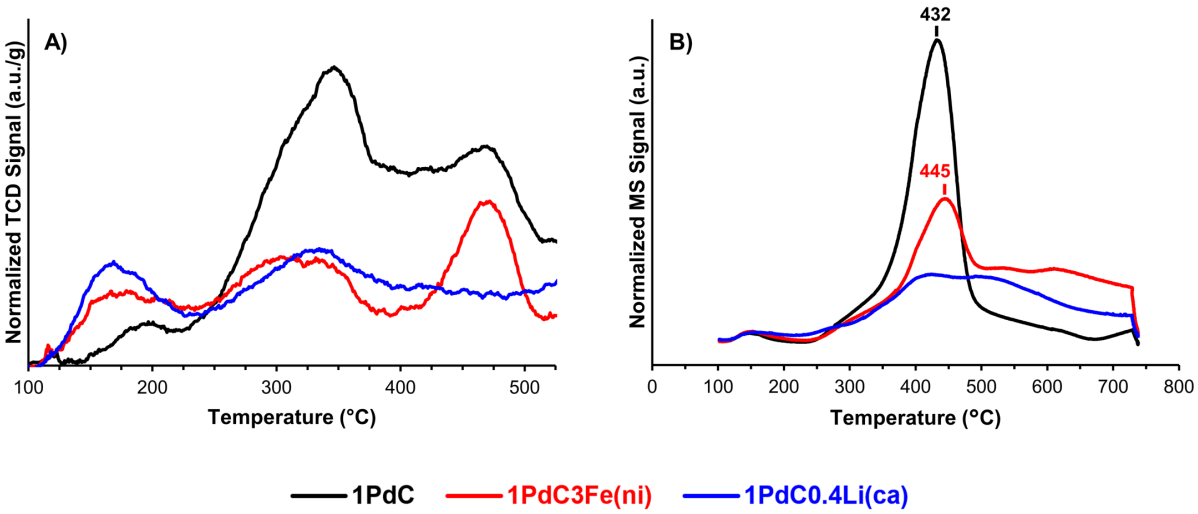

Figure 3. A) NH_3-TPD (samples were reduced in-situ at 200 °C-50 ml/min H_2 for 1 h before analysis) and B) H_2-TPD (background corrected for H_2 desorbed from the support) profiles of Pd, PdFe, and PdLi catalysts

Unfortunately, the low metal loadings used here did not allow meaningful XPS results to be obtained. Therefore, an etching technique was used to remove SiO_2 and enhance the weight percentage of metals in the samples as to enable data collection using XPS. **Figure 4** shows Pd 3d spectra of the samples after etching with 10% NaOH at 80 °C to remove SiO_2. A clear shift to lower binding energies of ~0.3 eV was observed after the incorporation of Fe. This suggested a charge transfer from Fe to Pd resulting in increased electron density of the Pd, which would lead to enhanced interaction with the AP/PE oxygen atoms. The transfer of electron density from Fe to Pd was also observed by Kim et al., though they reported a much larger shift in binding energies of ~1 eV for PdFe compared to the monometallic catalyst.[35] A similar effect has been recently reported for a NiGa bimetallic system where XPS results indicated a charge transfer from Ga to Ni manifested as a slight shift (~0.2 eV) of the Ni $2P_{3/2}$ peak position.[71] Furthermore, peak fitting results displayed in **Figure S4** showed that, in addition to the binding energy shift, the PdFe sample had a higher ratio of Pd^{2+} to Pd^0 suggesting the presence of Fe led to some oxidation of the Pd particles likely due to the oxophilicity of Fe. These results indicated PdFe would have a higher affinity to oxygen, which could at least partially explain the higher selectivity to EB during the conversion of AP/PE.

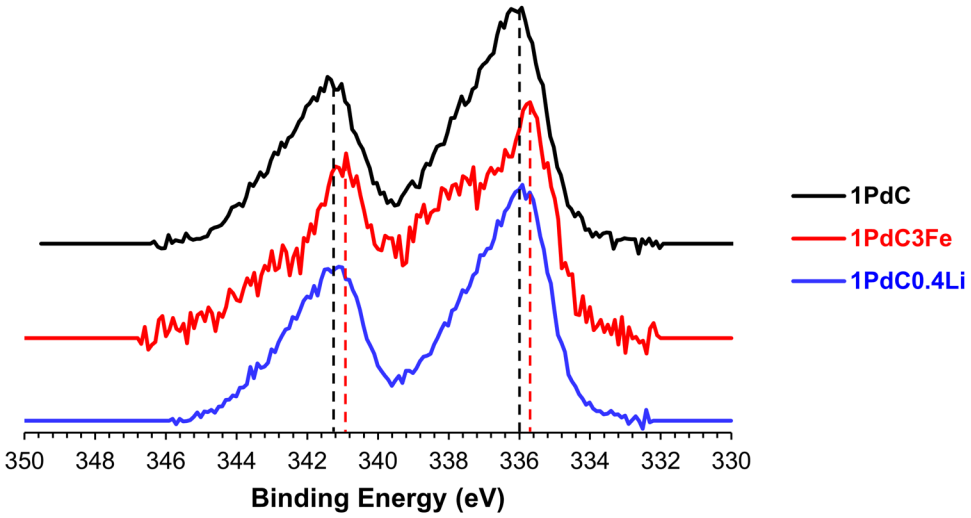

Figure 4. Pd 3d spectra of Pd, PdFe, and PdLi catalysts after etching with 10% NaOH (XPS spectra are normalized and baseline corrected)

Kim et al. used XPS to confirm the electronic effect of Fe on Pd atoms as a function of Fe/Pd ratio.[72] While the location of the Pd 3d peaks shifted to lower binding energies from Fe addition, at Fe/Pd ratios of 0.7 and higher, the electronic effect appeared to reach a plateau in agreement with the changes observed in product selectivity.[72] Conversely, Geng et al. found a Pd 3d shift to higher values for carbon nanofiber-supported PdFe compared to Pd catalysts,[73] which was in agreement with previous reports investigating the formation of PdFe alloys.[37, 74-76] Note that in these reports Pd and Fe particles were typically heated to 500-900 °C whereas in our work annealing and reduction took place only as high as 300 °C. Therefore, these differences might be explained by the formation of a different intermetallic phase in our study compared to those obtained in the above-mentioned investigations.

Next, magic-angle spinning (MAS) solid-state NMR spectroscopy was used to further probe structure within the heterogenous catalysts. Unless noted otherwise, all catalysts were impregnated with a thin-film (~2 nm) of AP or PE using a (AP) 0.2 or (PE) 0.27 M solution in fully deuterated ethanol to probe binding through ^{1}H NMR signal linewidths. The binding of AP or PE onto the surface of the catalysts will result in broadened ^{1}H NMR signals due to decreased dynamics; the ^{1}H NMR signals will narrow for weakly surface bound AP/PE and become solution like for AP or PE residing in the thin-film solution (~2 nm).[77-78] For example, previous work impregnating γ-alumina with bicyclic lactone in dioxane-d_8 (~130-200 mg/mL, ~2 nm film) showed that bicyclic lactone binds strongly to the hydrated γ-alumina surface.[78]

^{1}H MAS solid-state NMR spectra of C/Davisil (no Pd or co-metal) prepared with a thin-film solution of either AP or PE revealed broad ^{1}H NMR signals, suggesting that both AP and PE bind strongly to the surface of the carbon support (**Figure 5A** and **Figure S5**). Furthermore, the majority of aromatic and methyl ^{1}H NMR

signals for AP and PE both moved to a lower ^{1}H chemical shift by *ca.* 1.5-3 ppm than when just in a solution of ethanol-d_6. One-dimensional (1D) ^{1}H→^{13}C cross-polarization MAS (CPMAS) solid-state NMR spectra of C/Davisil and 1PdC both showed a broad ^{13}C NMR signal (FWHM ~ 20 ppm) centered at *ca.* 125 ppm that is typical of graphitic (sp^2-hybridized) carbon (**Figure 5B**).[31, 79-82] Of note is that the ^{13}C NMR spectra reported here were similar to that of other carbon-coated silica supported metal catalysts.[31, 81] The 1-3 ppm decrease in ^{1}H chemical shift observed for AP and PE was likely caused by *ring current effects* that result from the molecules (aromatic and/or C=O groups) lying across the graphitic carbon surface. Such *ring current effects*, where there is additional shielding of the nucleus (reduced local magnetic field) caused by circulation of delocalized surface carbon π electrons, have previously been observed experimentally and theoretically for small molecules absorbed onto carbons.[83-85] Therefore, it can be concluded that the aromatic and C=O groups of AP and PE both strongly adsorb to the graphitic carbon surface of the support, even in the absence of Pd or another co-metal. Not surprisingly, AP and PE also bind strongly to the catalysts when there is PdLi or just Pd on the support, respectively (**Figure 5A** and **Figure S5**). AP or PE binding onto PdFe was not probed due to the paramagnetic nature of Fe. Indeed, a ^{1}H NMR spectrum of PdFe (no thin film) revealed significantly broadened surface ^{1}H NMR signals with a large spinning sideband manifold that spans a breadth of greater than 500 ppm (**Figure S6**). The broad ^{1}H spinning sideband manifold likely arose from strong nuclear-electron dipolar couplings between unpaired electrons associated with Fe ions and the surface ^{1}H spins.[86-88] The fact there were no narrow ^{1}H NMR signals suggested that Fe ions were likely homogeneously dispersed across the surface of the catalyst.

Unfortunately, more complex heteronuclear and/or homonuclear correlation NMR experiments could not be used to reliably assign the binding strength or further probe interaction of AP/PE with the carbon support or metal particles because ethanol-d_6 started to evaporate from the NMR rotor when spinning for longer periods of time (**Figure S7**). All the thin-film ^{1}H NMR spectra shown were recorded within *ca.* 10 minutes of spinning in order to limit solvent evaporation. However, direct excitation ^{7}Li solid-state NMR spectrum of PdLi revealed two distinct ^{7}Li NMR signals centered at *ca.* 0 ppm with different linewidths (**Figure 5C**). Based on the ^{7}Li chemical shift of *ca.* 0 ppm, a significant fraction of Li atoms exist as diamagnetic ions. The two ^{7}Li NMR signals only differed by means of linewidths. The broad ^{7}Li NMR signal likely corresponded to immobilized/surface supported diamagnetic Li, while the narrow ^{7}Li NMR signal could be attributed to diamagnetic Li with a higher degree of mobility on the support surface. Finally, it is noted that the lack of ^{7}Li NMR signals exhibiting shifts typical of metallic Li does not imply the absence of alloying Pd, rather it is likely the these ^{7}Li NMR signals could be broadened beyond detection, especially as compared to the much narrower signal from diamagnetic Li ions.

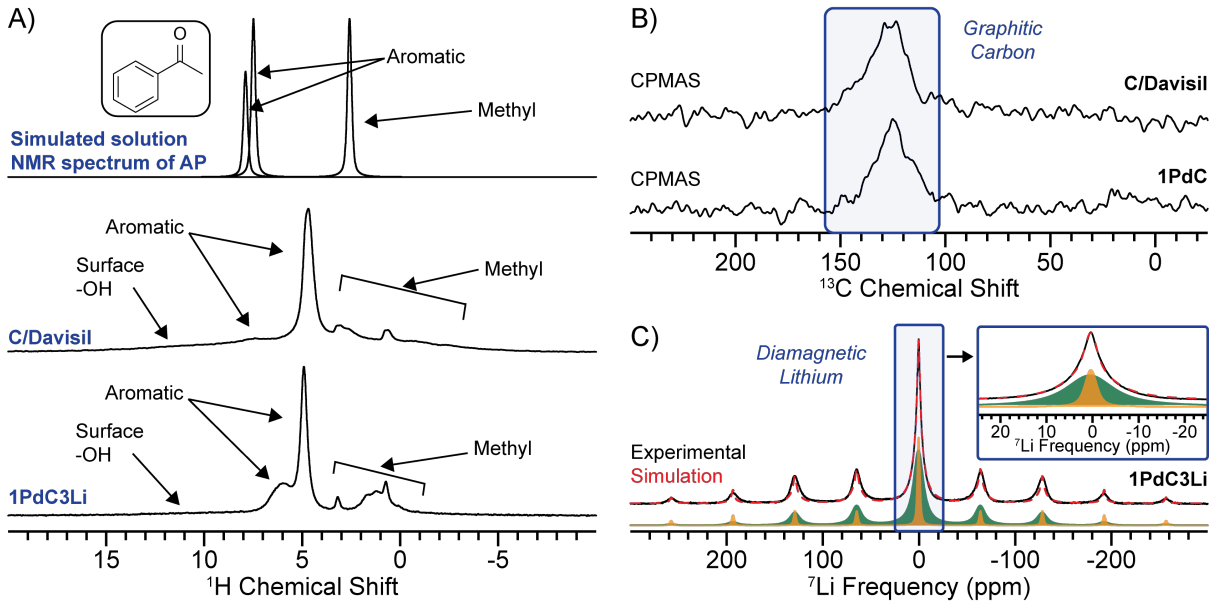

Figure 5. (A) ^{1}H solution NMR spectrum of AP in ethanol-d_6 recorded at B_0 = 14.1 T. The red # indicates solvent ^{1}H NMR signals. (Lower) 1D direct excitation ^{1}H MAS solid-state NMR spectra of C/Davisil and 1PdC3Li impregnated with a thin-film (~ 2 nm) solution of AP in ethanol-d_6 (~ 0.2 M). Note that the ^{1}H MAS NMR spectra were recorded within 10 minutes of spinning the NMR rotor. (B) ^{1}H→^{13}C CPMAS NMR spectra of (upper) C/Davisil and (lower) 1PdC. (C) Direct excitation ^{7}Li spin echo NMR spectrum of 1PdC3Li. The (solid) black and (dashed) red lines correspond to experimental and analytical simulated NMR spectra. Inset shows isotropic ^{7}Li NMR signals, while higher and lower frequency signals are spinning sidebands. All solid-state NMR spectra were recorded at B_0 = 9.4 T (ν_0(^{1}H) = 400 MHz) with 10 kHz MAS.

Catalytic reactions

The results of the AP and PE reactions are shown in **Table 2**. As shown in **Scheme 1**, AP could hydrogenate to either PE or CMK in parallel. While CMK did not react any further, PE could dehydrogenate back to AP, hydrogenate to form CE, or deoxygenate to yield EB. CE would be considered a terminal product since it did not react further, but EB could hydrogenate to EC. Using the Pd monometallic catalyst, a relatively similar distribution of final products was obtained from both feedstocks. Conversely, PdLi and PdFe resulted in significantly different product distributions. The PdFe catalyst favored the deoxygenation pathway to produce EB with a selectivity of more than 95% among the final products, whereas PdLi noticeably favored the aromatic hydrogenation pathway with more than 93% selectivity to CMK and CE among the final products (i.e., EB, CMK, CE, EC).

It should be noted that our catalytic results were not optimized, meaning that the ratio of Pd to co-metal, operating conditions, and the synthesis method were not tuned to maximize the selectivity. In addition to the mentioned parameters a potential way to further enhance the selectivity of products using the interaction between Pd and co-metal particles would be to use selective synthesis methods such as the one used by Ro et al.[89]

Table 2. Conversion and product selectivity of AP and PE over Pd, PdFe, and PdLi catalysts [a]

Catalyst	Feed	Conv. (C%)	Selectivity (C%)				
			EC	EB	CE	CMK	PE / AP
1PdC [b]	AP	77	6.6	28.5	18.0	20.0	26.9
1PdC3Fe [b]		59	0	54.3	0.3	0.8	44.6
1PdC3Li [b]		62	0	1.8	9.6	27.0	61.6
1PdC	PE	53	6.1	48.5	23.7	18.7	3.0
1PdC3Fe		53	0.5	96.6	0.2	0.1	2.6
1PdC0.4Li		26	0.2	7.4	38.4	46.5	7.6
1PdC3Li		17	0	5.6	35.5	44.7	14.1

[a]: Reaction conditions: 10 mg catalyst, 100 ml/min H_2, 0.2 ml/min feeding rate, 0.2 M AP or PE in ethanol, 200 °C, 5 MPa. [b]: 20 mg catalyst was used in AP reactions instead of 10 mg.

Although likely more complicated due to the presence of feed and solvent molecules under the reaction conditions, according to P-C-T relationships reported for Pd-H systems, Pd hydrides could be formed at 200 °C and 5 MPa.[69] Therefore, if Li was indeed occupying the interstitial sites of the Pd lattice as suggested by the H_2-TPD data then it could be postulated that Pd hydrides are important for the hydrogenolysis of C-OH bonds in PE, whereas surface-bound H atoms were responsible for hydrogenating the π bonds in C=O and the aromatic ring. This was supported by similar conversions observed over PdLi and Pd catalysts for the AP feed (with a much higher selectivity to PE in the case of PdLi), while considerably lower conversions were obtained over PdLi catalysts when PE was used as the feed. The differences in reactivity of bulk (interstitial) and surface-bound H resulting from different energy states of these two species and adsorbate interaction have been previously discussed, especially in the context of selective hydrogenation of acetylene to ethylene.[90, 91] Similarly, the Li incorporation into the Pd lattice has been reported to occupy the interstitial sites denying access to hydrogen and preventing the formation of Pd hydrides, resulting in Pd lattice expansion and modification of electronic properties of Pd NPs, which eventually affected the selectivity of hydrogenation reactions.[70]

PdFe bimetallic catalysts have been shown to have a higher activity for hydrogenation of C=O bonds than a single metallic Pd catalyst, demonstrated by a higher apparent turnover frequency for acetone hydrogenation to isopropanol under similar conditions to this work.[3] The lattice d-spacing measured by high-resolution TEM images and the H_2-TPD profiles suggested the existence of a PdFe intermetallic phase. The higher intrinsic activity of Pd particles in the presence of Fe (based on CO chemisorption) was attributed to this electronic effect. Similarly, PdFe bimetallic systems have been identified to selectively catalyze hydrogenolysis reactions without aromatic ring hydrogenation for aromatic ethers typically found in biopolymers.[35, 72, 92] Kim et al. attributed the higher selectivity of PdFe catalysts to aromatics (as opposed to cycloalkanes for Pd catalyst) to its modified electronic properties as suggested by XPS, XRD, H_2-TPR, and H_2-TPD results.[35, 72] The addition of Fe to Pd (and its ratio) was also found to affect the selectivity of citral hydrogenation.[92]

The duration of catalyst reduction before the reactions had no effect on conversion or product selectivity (**Figure S8**) indicating that the catalysts were reduced rapidly under the reaction conditions, i.e., 200 °C and 5 MPa H_2 as expected from Pd NPs.

Both conversion and selectivity to EB enhanced when 2% D_2O was added to the feed solution for the Pd and PdLi catalysts, but no changes were observed for PdFe (**Figure S9**). Mass spectrometry results suggested that there are two hydrogenation pathways. One is hydrogenation using molecular H_2 and the other is hydrogenation by water (D_2O) molecules. The contribution from water was substantially smaller than molecular hydrogen but considering the low concentration of D_2O (2% in ethanol) it could mean that if these reactions were done in water, product selectivity would have been different.

Finally, the effect of co-metal intimacy on conversion and product selectivity was investigated by conducting reactions using physical mixtures of Pd (no co-metal) and Fe (no Pd) samples as well as Pd and Li samples. The results are presented in **Figure 6**. These results suggested that intimate contact between Fe or Li and Pd played an important role in product distribution. The results for Pd+Fe were similar to the Pd results suggesting that the intimacy between Fe and Pd particles was necessary for high EB selectivity obtained using the PdFe catalyst, which is in line with the electron transfer between Pd and Fe observed via XPS. In contrast, the physical mixture of Pd+Li resulted in a lower selectivity to EB compared with 1PdC but higher compared to PdLi. In agreement with our NMR investigation suggesting the presence of both anchored and mobile Li species on the support, this could indicate leaching of mobile Li particles during the reaction and the formation of PdLi phases leading to higher selectivity to CMK and CE. Tabular data for these graphs are available in the ESI (**Table S3**).

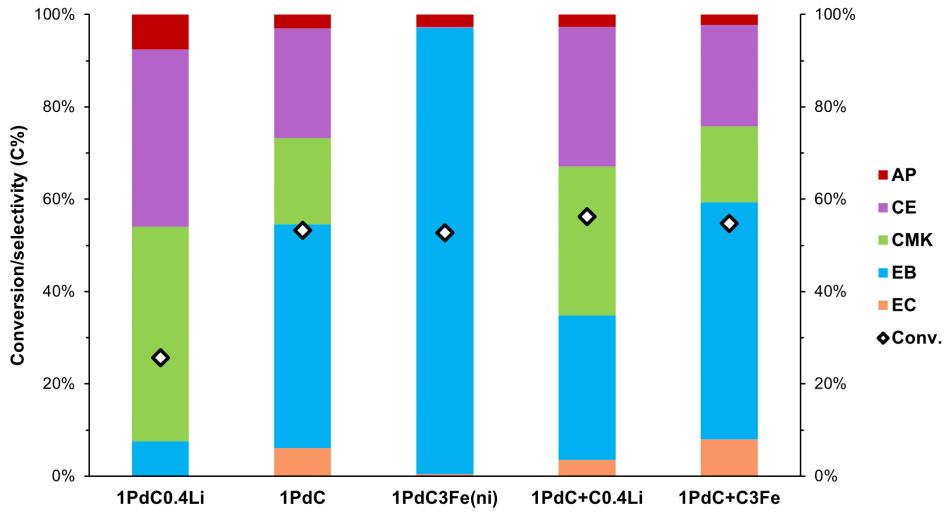

Figure 6. The effect of co-metal intimacy with Pd on the conversion of PE (10 mg catalyst, 100 ml/min H_2, 0.2 ml/min feeding rate, 0.2 M PE in ethanol, 200 °C, 5 MPa)

DFT calculations

DFT calculations were conducted to evaluate the energetics of AP hydrogenation on representative Pd, PdFe and PdLi catalyst models. The intermediates considered in the reaction network corresponding to elementary hydrogenation events are depicted in **Figure S11**. The adsorbate orientation and binding site preference were controlled by the relatively strong metal-oxygen interactions. For example, in AP, the nearest metal (M)-O distance and the average distance of the aromatic carbon are provided (**Figure S12**) along with their respective adsorption energies on each of the metal surfaces. Due to the oxophilic nature of Fe, the strong Fe-O interaction enhanced the adsorption of AP on the $Pd_3Fe(111)$ surface (-2.12 eV) relative to $Pd_H(111)$ and $Pd_{Li}(111)$ surfaces (-2.03 eV and -1.64 eV, respectively). In the Li case, there was likely minor transfer of electron density from Li atoms to the Pd atoms on the top surface (~10%) as observed in a previous study,[43] thereby stabilizing the Pd surface leading to weak chemisorption of the adsorbate on the surface. These variations in the adsorbate-surface interactions have important impacts on hydrogenation energetics and corresponding selectivities to products formed by hydrogenation of C=C (ring) and C=O bonds.

In **Figure 7**, the free energies of elementary hydrogenation steps are compared to elucidate reasons for the observed reaction product selectivity based on thermochemistry on $Pd_H(111)$, $Pd_3Fe(111)$, and $Pd_{Li}(111)$. The free energies of all surface intermediates can be found in **Table S4**. Considered in the calculations were initial hydrogen addition to ortho, meta, and para positions of the rings; addition at ortho sites was found to be most favorable in all cases and is therefore reported here.

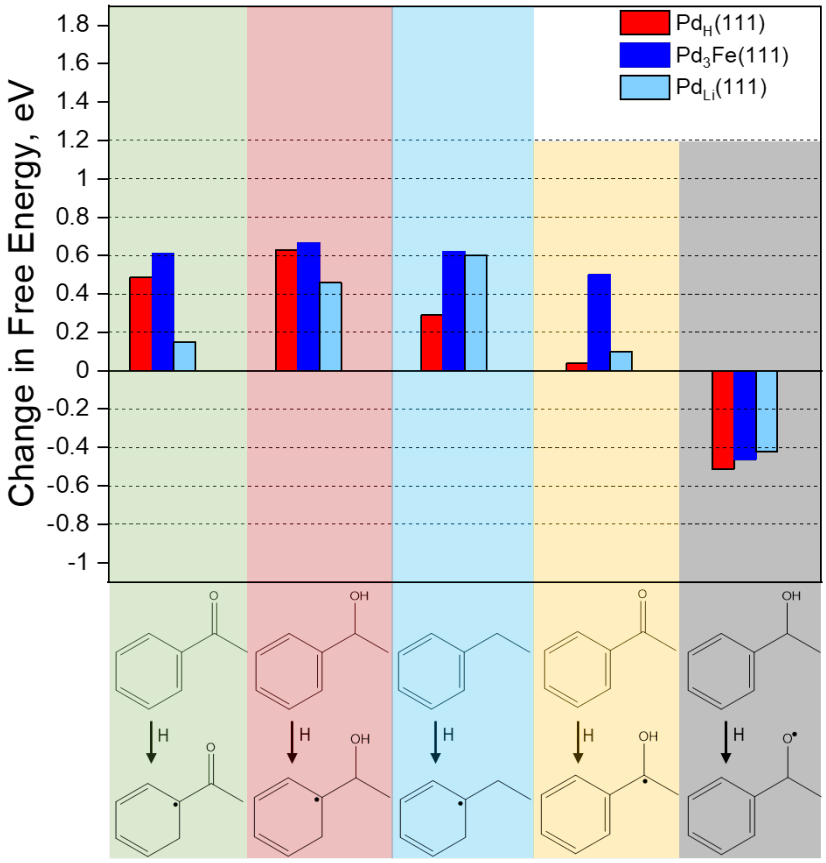

Figure 7. Calculated free energies of the first elementary H-addition step of AP (green shadow), PE (pink), and EB (blue) ring hydrogenation; AP (yellow) carbonyl hydrogenation, and PE (grey) carbonyl hydrogenolysis at 200 °C and 5 MPa.

In general, for all cases modeled, the aromatic ring hydrogenation and carbonyl hydrogenation at C in C=O moiety were endergonic while the carbonyl hydrogenolysis was exergonic. The $Pd_H(111)$ surface was used as a base case for understanding the relative effects of adding Fe and Li, and to examine the energetics on the alloy surfaces relative to those on $Pd_H(111)$. The analysis was focused on the first hydrogenation event of each closed-shell species, as it should be anticipated to offer a rough indicator of the relative difficulties of full hydrogenation.

The $Pd_3Fe(111)$ surface demonstrated the oxophilic nature of Fe as evident from the shortened metal-oxygen distance (**Figure S12**). As shown in **Figure 7**, the initiation of ring hydrogenation was less favorable than on $Pd_H(111)$ (0.61 eV vs 0.49 eV), with higher free energies required to add H to any of the three closed-shell aromatic species. Therefore, more difficult kinetics were inferred for these H-addition steps on PdFe, following the well-known Brønsted-Evans-Polanyi relationships in heterogenous catalysis,[93] providing a potential explanation for the experimentally observed reduction in ring hydrogenation on PdFe. A higher reaction free energy was calculated for carbonyl hydrogenation and subsequent hydrogenolysis on $Pd_3Fe(111)$ than on $Pd_H(111)$, which seemed contradictory to the improved experimental selectivity to EB on PdFe. We however rationalize the experimentally observed

facile hydrogenation and hydrogenolysis considering geometric effects and subsequent kinetic favorability due to the exceptionally strong adsorption of the carbonyl moiety to surface Fe atoms, making the C=O or C-OH moieties more accessible to surface-bound H.

Calculations of the first elementary hydrogenation on the $Pd_{Li}(111)$, in contrast, showed enhanced energetic favorability for ring hydrogenation (**Figure 7**), consistent with the experimental results. The first hydrogenation of AP (toward CMK) and PE (toward CE) on $Pd_{Li}(111)$ were notably less endothermic than on $Pd_H(111)$, consistent with the increased production of CMK and CE on the PdLi catalyst. The first ring hydrogenation of EB, however, was more unfavorable than on $Pd_H(111)$ (0.60 eV vs 0.29 eV), consistent with the lack of EC observed on PdLi. Like the $Pd_3Fe(111)$ model, the $Pd_{Li}(111)$ surface demonstrated more unfavorable energetics of carbonyl hydrogenation than on $Pd_H(111)$. However, in contrast to $Pd_3Fe(111)$, we did not observe strong binding of the carbonyl so we infer there is no kinetic enhancement relative to $Pd_H(111)$. Together, these suggest fundamental reasons for the selectivity observed on the PdLi catalyst.

Conclusion

Chemoselective hydrogenation of aromatic ketones is of great significance in the pharmaceutical and specialty chemical industries. Selective hydrogenation or hydrodeoxygenation of multifunctional molecules is also important for product diversification from bio-based molecules. In this work, we found that through the addition of co-metals to Pd, the product distribution could be significantly altered. Using acetophenone or 1-phenylethanol feeds, the monometallic Pd catalyst produced an almost even distribution of products. PdFe exclusively produced ethylbenzene (95+%), which was attributed to either modified electronic properties of the Pd NPs (according to XPS results) or enhanced geometric effects on C=O adsorption (based on DFT calculations). DFT calculations additionally showed the unfavorability of initiating ring hydrogenation on PdFe, along with more favorable binding/activation of the carbonyl group to the surface. PdLi preferred the hydrogenation of the phenyl group to form cyclohexylmethylketone and cyclohexylethanol with an unprecedented selectivity over hydrodeoxygenation to ethylbenzene. The near absence of Pd hydride phases in the PdLi catalyst as evidenced from H_2-TPD data simultaneously with low deoxygenation rates suggest the role of Pd-H phases in C-OH cleavage, which could be due to higher energetics of bulk H compared to surface H affecting the electronic properties of the Pd NPs.

Our synthesis approach enabled screening of various bimetallic systems in technical grade catalysts for our model reaction. Further studies with model catalysts are required to more definitively validate our proposed mechanisms. The applicability of these bimetallic systems to other bio-based molecules could help in selective product diversification of biomass-derived molecules and open new venues for bio-advantaged molecules.[11]

Supporting Information

The Supporting Information is available online and includes detailed descriptions of the experimental and computational methods; TEM images, NH_3-TPD profiles, XPS and NMR characterization; additional reaction results; basis for computational results.

Acknowledgements

The authors would like to thank Alex Kaufmann and Zachary Alston for performing many of the reaction experiments. The authors would also like to acknowledge funding from the Mike and Jean Steffenson Chair and the Michael and Denise Mack Faculty Fellowship. Solid-state NMR spectroscopy (R.W.D. and A.J.R.) was supported by the National Science Foundation under Grant CBET-1916809. We are thankful to Dapeng Jing for performing XPS experiments and Patrick Johnston for ICP analysis.

References

1. De, S.; Saha, B.; Luque, R., Hydrodeoxygenation Processes: Advances on Catalytic Transformations of Biomass-Derived Platform Chemicals into Hydrocarbon Fuels. *Bioresour. Tech.* **2015**, *178*, 108-118. DOI: 10.1016/j.biortech.2014.09.065
2. Gilkey, M. J.; Xu, B., Heterogeneous Catalytic Transfer Hydrogenation as an Effective Pathway in Biomass Upgrading. *ACS Catal.* **2016**, *6*, 1420-1436. DOI: 10.1021/acscatal.5b02171
3. Sievers, C.; Noda, Y.; Qi, L.; Albuquerque, E. M.; Rioux, R. M.; Scott, S. L., Phenomena Affecting Catalytic Reactions at Solid–Liquid Interfaces. *ACS Catal.s* **2016**, *6*, 8286-8307. DOI: 10.1021/acscatal.6b02532
4. Besson, M. I.; Gallezot, P.; Pinel, C., Conversion of Biomass into Chemicals over Metal Catalysts. *Chem. Rev.* **2014**, *114*, 1827-1870. DOI: 10.1021/cr4002269
5. Blaser, H. U.; Malan, C.; Pugin, B.; Spindler, F.; Steiner, H.; Studer, M., Selective Hydrogenation for Fine Chemicals: Recent Trends and New Developments. *Adv. Synth. Catal.* **2003**, *345*, 103-151. DOI: 10.1002/adsc.200390000
6. Machado, R. M.; Heier, K. R.; Broekhuis, R. R., Developments in Hydrogenation Technology for Fine-Chemical and Pharmaceutical Applications. *Curr. Opin. Drug Discov. Dev.* **2001**, *4*, 745-755. DOI:10.1002/CHIN.200218253
7. Klingler, F. D., Asymmetric Hydrogenation of Prochiral Amino Ketones to Amino Alcohols for Pharmaceutical Use. *Acc. Chem. Res.* **2007**, *40*, 1367-1376. DOI: 10.1021/ar700100e
8. Rautanen, P. A.; Lylykangas, M. S.; Aittamaa, J. R.; Krause, A. O. I., Liquid-Phase Hydrogenation of Naphthalene and Tetralin on Ni/Al_2O_3: Kinetic Modeling. *Ind. Eng. Chem. Res.* **2002**, *41*, 5966-5975. DOI: 10.1021/ie020395q
9. Toppinen, S.; Salmi, T.; Rantakylä, T. K.; Aittamaa, J., Liquid-Phase Hydrogenation Kinetics of Aromatic Hydrocarbon Mixtures. *Ind. Eng. Chem. Res.* **1997**, *36*, 2101-2109. DOI: 10.1021/ie960263v
10. Al Obaidi, Y.; Kozminski, M.; Ward, J.; Johnson, M.; Guevremont, J. M., Hydrodearomatization of Distillates and Heavy Naphtha over a Precious Metal Hydrogenation Catalyst and the Determination of Low Aromatic Content. *Ind. Eng. Chem. Res.* **2018**, *57*, 12029-12035. DOI: 10.1021/acs.iecr.8b02909
11. Shanks, B. H.; Keeling, P. L., Bioprivileged Molecules: Creating Value from Biomass. *Green Chem.* **2017**, *19*, 3177-3185. DOI: 10.1039/C7GC00296C
12. Zhang, L.; Zhou, M.; Wang, A.; Zhang, T., Selective Hydrogenation over Supported Metal Catalysts: From Nanoparticles to Single Atoms. *Chem. Rev.* **2019**, *120*, 683-733. DOI: 10.1021/acs.chemrev.9b00230
13. Shimazu, S.; Baba, N.; Ichikuni, N.; Uematsu, T., Regioselective Hydrogenation of Dienes Catalyzed by Palladium–Aminosilane Complexes Grafted on MCM-41. *J. Molec. Catal. A: Chem.* **2002**, *182*, 343-350. DOI: 10.1016/S1381-1169(01)00508-8

14. Panpranot, J.; Pattamakomsan, K.; Praserthdam, P.; Goodwin, J. G., Impact of the Silica Support Structure on Liquid-Phase Hydrogenation on Pd Catalysts. *Ind. Eng. Chem. Res.* **2004**, *43*, 6014-6020. DOI: 10.1021/ie0497947
15. Wei, Y.; Rao, B.; Cong, X.; Zeng, X., Highly Selective Hydrogenation of Aromatic Ketones and Phenols Enabled by Cyclic (Amino)(alkyl)carbene Rhodium Complexes. *J. Amer. Chem. Soc.* **2015**, *137*, 9250-9253. DOI: 10.1021/jacs.5b05868
16. Wang, R.; Li, Y.; Shi, R.; Yang, M., Effect of Metal–Support Interaction on the Catalytic Performance of Ni/Al_2O_3 for Selective Hydrogenation of Isoprene. *J. Molec. Catal. A: Chem.* **2011**, *344*, 122-127. DOI: 10.1016/j.molcata.2011.05.009
17. Pagán-Torres, Y. J.; Gallo, J. M. R.; Wang, D.; Pham, H. N.; Libera, J. A.; Marshall, C. L.; Elam, J. W.; Datye, A. K.; Dumesic, J. A., Synthesis of Highly Ordered Hydrothermally Stable Mesoporous Niobia Catalysts by Atomic Layer Deposition. *ACS Catal.* **2011**, *1*, 1234-1245. DOI: 10.1021/cs200367t
18. Ravenelle, R. M.; Copeland, J. R.; Kim, W.-G.; Crittenden, J. C.; Sievers, C., Structural Changes of γ-Al_2O_3-Supported Catalysts in Hot Liquid Water. *ACS Catal.* **2011**, *1*, 552-561. DOI: 10.1021/cs1001515
19. Jongerius, A. L.; Copeland, J. R.; Foo, G. S.; Hofmann, J. P.; Bruijnincx, P. C. A.; Sievers, C.; Weckhuysen, B. M., Stability of Pt/γ-Al_2O3 Catalysts in Lignin and Lignin Model Compound Solutions under Liquid Phase Reforming Reaction Conditions. *ACS Catal.* **2013**, *3*, 464-473. DOI: 10.1021/cs300684y
20. Sankar, M.; Dimitratos, N.; Miedziak, P. J.; Wells, P. P.; Kiely, C. J.; Hutchings, G. J., Designing Bimetallic Catalysts for a Green and Sustainable Future. *Chem. Soc. Rev.* **2012**, *41*, 8099-8139. DOI: 10.1039/C2CS35296F
21. Tomishige, K.; Nakagawa, Y.; Tamura, M., Selective Hydrogenolysis and Hydrogenation Using Metal Catalysts Directly Modified with Metal Oxide Species. *Green Chem.* **2017**, *19*, 2876-2924. DOI: 10.1039/C7GC00620A
22. Cuenya, B. R.; Behafarid, F., Nanocatalysis: Size-and Shape-Dependent Chemisorption and Catalytic Reactivity. *Surf. Sci. Rep.* **2015**, *70*, 135-187. DOI: 10.1016/j.surfrep.2015.01.001
23. Liu, L.; Corma, A., Metal Catalysts for Heterogeneous Catalysis: From Single Atoms to Nanoclusters and Nanoparticles. *Chem. Rev.* **2018**, *118*, 4981-5079. DOI: 10.1021/acs.chemrev.7b00776
24. Kulagina, M. A.; Simonov, P. A.; Gerasimov, E. Y.; Kvon, R. I.; Romanenko, A. V., To the Nature of the Support Effect in Palladium-Catalyzed Aqueous-Phase Hydrogenation of Maleic Acid. *Colloids Surf. A Physicochem. Eng. Asp.* **2017**, *526*, 29-39. DOI: 10.1016/j.colsurfa.2016.11.037
25. Coq, B.; Figueras, F., Bimetallic Palladium Catalysts: Influence of the Co-Metal on the Catalyst Performance. *J. Molec. Catal. A: Chem.* **2001**, *173*, 117-134. DOI: 10.1016/S1381-1169(01)00148-0
26. Cheng, Y.; Pham, H.; Huo, J.; Johnson, R.; Datye, A. K.; Shanks, B., High Activity Pd-Fe Bimetallic Catalysts for Aqueous Phase Hydrogenations. *Molec. Catal.* **2019**, *477*, 110546. DOI: 10.1016/j.mcat.2019.110546
27. Vetere, V.; Merlo, A. B.; Ruggera, J. F.; Casella, M. L., Transition Metal-Based Bimetallic Catalysts for the Chemoselective Hydrogenation of Furfuraldehyde. *J. Braz. Chem. Soc.* **2010**, *21*, 914-920. DOI: 10.1590/S0103-50532010000500021
28. Wang, A.; Liu, X. Y.; Mou, C.-Y.; Zhang, T., Understanding the Synergistic Effects of Gold Bimetallic Catalysts. *J. Catal.* **2013**, *308*, 258-271. DOI: 10.1016/j.jcat.2013.08.023
29. Xin, H.; Holewinski, A.; Schweitzer, N.; Nikolla, E.; Linic, S., Electronic Structure Engineering in Heterogeneous Catalysis: Identifying Novel Alloy Catalysts Based on Rapid Screening for Materials with Desired Electronic Properties. *Top. Catal.* **2012**, *55*, 376-390. DOI: 10.1007/s11244-012-9794-2
30. Bravo-Suárez, J. J.; Chaudhari, R. V.; Subramaniam, B., Design of Heterogeneous Catalysts for Fuels and Chemicals Processing: An Overview. In *Novel Materials for Catalysis and Fuels Processing*, ACS Publications: **2013**, 3-68.
31. Pham, H. N.; Anderson, A. E.; Johnson, R. L.; Schwartz, T. J.; O'Neill, B. J.; Duan, P.; Schmidt-Rohr, K.; Dumesic, J. A.; Datye, A. K., Carbon Overcoating of Supported Metal Catalysts for Improved Hydrothermal Stability. *ACS Catal.* **2015**, *5*, 4546-4555. DOI: 10.1021/acscatal.5b00329
32. Xiong, H.; Pham, H. N.; Datye, A. K., Hydrothermally Stable Heterogeneous Catalysts for Conversion of Biorenewables. *Green Chem.y* **2014**, *16*, 4627-4643. DOI: 10.1039/C4GC01152J
33. Joo, S. H.; Choi, S. J.; Oh, I.; Kwak, J.; Liu, Z.; Terasaki, O.; Ryoo, R., Ordered Nanoporous Arrays of Carbon Supporting High Dispersions of Platinum Nanoparticles. *Nature* **2001**, *412*, 169-172. DOI: 10.1038/35084046

34. Li, T.; Ji, N.; Jia, Z.; Diao, X.; Wang, Z.; Liu, Q.; Song, C.; Lu, X., Effects of Metal Promoters in Bimetallic Catalysts in Hydrogenolysis of Lignin Derivatives into Value-Added Chemicals. *ChemCatChem* **2020**, *12*, 5288-5302. DOI: 10.1002/cctc.202001124
35. Kim, J. K.; Lee, J. K.; Kang, K. H.; Song, J. C.; Song, I. K., Selective Cleavage of CO Bond in Benzyl Phenyl Ether to Aromatics over Pd–Fe Bimetallic Catalyst Supported on Ordered Mesoporous Carbon. *Appl. Catal. A: Gen.* **2015**, *498*, 142-149. DOI: 10.1016/j.apcata.2015.03.034
36. Xiang, Y.-Z.; Lv, Y.-A.; Xu, T.-Y.; Li, X.-N.; Wang, J.-G., Selectivity Difference between Hydrogenation of Acetophenone over CNTs and ACs Supported Pd Catalysts. *J. Molec. Catal. A: Chem.* **2011**, *351*, 70-75. DOI: 10.1016/j.molcata.2011.09.018
37. Pino, N.; Sitthisa, S.; Tan, Q.; Souza, T.; López, D.; Resasco, D. E., Structure, Activity, and Selectivity of Bimetallic Pd-Fe/SiO_2 and Pd-Fe/γ-Al_2O_3 Catalysts for the Conversion of Furfural. *J. Catal.* **2017**, *350*, 30-40. DOI: 10.1016/j.jcat.2017.03.016
38. Sun, J.; Karim, A. M.; Zhang, H.; Kovarik, L.; Li, X. S.; Hensley, A. J.; McEwen, J.-S.; Wang, Y., Carbon-Supported Bimetallic Pd–Fe Catalysts for Vapor-Phase Hydrodeoxygenation of Guaiacol. *J. Catal.* **2013**, *306*, 47-57. DOI: 10.1016/j.jcat.2013.05.020
39. Hensley, A. J.; Zhang, R.; Wang, Y.; McEwen, J.-S., Tailoring the Adsorption of Benzene on PdFe Surfaces: A Density Functional Theory Study. *J. Phys. Chem. C* **2013**, *117*, 24317-24328. DOI: 10.1021/jp406425q
40. Nørskov, J. K.; Abild-Pedersen, F.; Studt, F.; Bligaard, T., Density Functional Theory in Surface Chemistry and Catalysis. *Proc. Nat. Acad. Sci.* **2011**, *108*, 937-943. DOI: 10.1073/pnas.1006652108
41. Ashwell, A. P.; Lin, W.; Hofman, M. S.; Yang, Y.; Ratner, M. A.; Koel, B. E.; Schatz, G. C., Hydrogenation of Co to Methanol on Ni(110) through Subsurface Hydrogen. *J. Amer. Chem. Soc.* **2017**, *139*, 17582-17589. DOI: 10.1021/jacs.7b09914
42. Ellis, I. T.; Wolf, E. H.; Jones, G.; Lo, B.; Li, M. M.-J.; York, A. P.; Tsang, S. C. E., Lithium and Boron as Interstitial Palladium Dopants for Catalytic Partial Hydrogenation of Acetylene. *Chem. Commun.* **2017**, *53*, 601-604. DOI: 10.1039/C6CC08404D
43. Gelatt Jr, C.; Williams, A.; Moruzzi, V., Theory of Bonding of Transition Metals to Nontransition Metals. *Phys. Rev. B* **1983**, *27*, 2005. DOI: 10.1103/PHYSREVB.27.2005
44. Kepp, K. P., A Quantitative Scale of Oxophilicity and Thiophilicity. *Inorg. Chem.* **2016**, *55*, 9461-9470. DOI: 10.1021/acs.inorgchem.6b01702
45. Kresse, G.; Furthmüller, J., Efficient Iterative Schemes for Ab Initio Total-Energy Calculations Using a Plane-Wave Basis Set. *Phys. Rev.B* **1996**, *54*, 11169. DOI: 10.1103/physrevb.54.11169
46. Kresse, G.; Furthmüller, J., Efficiency of Ab-Initio Total Energy Calculations for Metals and Semiconductors Using a Plane-Wave Basis Set. *Comput. Mater. Sci.* **1996**, *6*, 15-50. DOI: 10.1016/0927-0256(96)00008-0
47. Blöchl, P. E., Projector Augmented-Wave Method. *Phys. Rev..B* **1994**, *50*, 17953. DOI: 10.1103/PhysRevB.50.17953
48. Klimeš, J.; Bowler, D. R.; Michaelides, A., Chemical Accuracy for the Van Der Waals Density Functional. *J. Phys. Condens. Matter* **2009**, *22*, 022201. DOI: 10.1088/0953-8984/22/2/022201
49. Klimeš, J.; Bowler, D. R.; Michaelides, A., Van Der Waals Density Functionals Applied to Solids. *Phys. Rev. B* **2011**, *83*, 195131. DOI: 10.48550/arXiv.1102.1358
50. Morin, C.; Simon, D.; Sautet, P., Intermediates in the Hydrogenation of Benzene to Cyclohexene on Pt(111) and Pd(111): A Comparison from DFT Calculations. *Surf. Sci.* **2006**, *600*, 1339-1350. DOI: 10.1016/j.susc.2006.01.033
51. Haynes, W. M., *CRC Handbook of Chemistry and Physics*; CRC press, 2014.
52. Yang, F.; Hellman, O.; Lucas, M.; Smith, H.; Saunders, C.; Xiao, Y.; Chow, P.; Fultz, B., Temperature Dependence of Phonons in Pd 3 Fe through the Curie Temperature. *Phys. Rev. B* **2018**, *98*, 024301. DOI: 10.1103/PhysRevB.98.024301
53. Monkhorst, H. J.; Pack, J. D., Special Points for Brillouin-Zone Integrations. *Phys. Rev. B* **1976**, *13*, 5188. DOI: 10.1103/PhysRevB.13.5188
54. Hiyoshi, N.; Sato, O.; Yamaguchi, A.; Shirai, M., Acetophenone Hydrogenation over a Pd Catalyst in the Presence of H_2O and CO_2. *Chem. Commun.* **2011**, *47*, 11546-11548. DOI: 10.1039/c1cc13130c
55. Drelinkiewicza, A.; Waksmundzka, A.; Makowski, W.; Sobczak, J. W.; Król, A.; Zieba, A., Acetophenone Hydrogenation on Polymer–Palladium Catalysts. The Effect of Polymer Matrix. *Catal. Lett.* **2004**, *94*, 143-156. DOI: 10.1023/B:CATL.0000020539.31128.d4

56. Kim, K. D.; Pokhrel, S.; Wang, Z.; Ling, H.; Zhou, C.; Liu, Z.; Hunger, M.; Mädler, L.; Huang, J., Tailoring High-Performance Pd Catalysts for Chemoselective Hydrogenation Reactions Via Optimizing the Parameters of the Double-Flame Spray Pyrolysis. *ACS Catal.* **2016**, *6*, 2372-2381. DOI: 10.1021/acscatal.6b00396
57. Chen, M.; Maeda, N.; Baiker, A.; Huang, J., Hydrogenation of Acetophenone on Pd/Silica–Alumina Catalysts with Tunable Acidity: Mechanistic Insight by in Situ Atr-Ir Spectroscopy. *ACS Catal.* **2018**, *8*, 6594-6600. DOI: 10.1021/acscatal.8b00169
58. Huang, J.; Jiang, Y.; Van Vegten, N.; Hunger, M.; Baiker, A., Tuning the Support Acidity of Flame-Made Pd/SiO_2–Al_2O_3 Catalysts for Chemoselective Hydrogenation. *J. Catal.* **2011**, *281*, 352-360. DOI: 10.1016/j.jcat.2011.05.023
59. Bejblová, M.; Zámostný, P.; Červený, L.; Čejka, J., Hydrogenation and Hydrogenolysis of Acetophenone. *Collect. Czechoslov. Chem. Commun.* **2003**, *68*, 1969-1984. DOI: 10.1135/CCCC20031969
60. Fujita, S.-i.; Onodera, Y.; Yoshida, H.; Arai, M., Selective Hydrogenation of Acetophenone with Supported Pd and Rh Catalysts in Water, Organic Solvents, and CO_2-Dissolved Expanded Liquids. *Green Chem.* **2016**, *18*, 4934-4940. DOI: 10.1039/C6GC00583G
61. Wang, Z.; Pokhrel, S.; Chen, M.; Hunger, M.; Mädler, L.; Huang, J., Palladium-Doped Silica–Alumina Catalysts Obtained from Double-Flame FSP for Chemoselective Hydrogenation of the Model Aromatic Ketone Acetophenone. *J. Catal.* **2013**, *302*, 10-19. DOI: 10.1016/j.jcat.2013.02.017
62. Yan, H.; Cheng, H.; Yi, H.; Lin, Y.; Yao, T.; Wang, C.; Li, J.; Wei, S.; Lu, J., Single-Atom Pd_1/Graphene Catalyst Achieved by Atomic Layer Deposition: Remarkable Performance in Selective Hydrogenation of 1, 3-Butadiene. *J. Amer. Chem. Society* **2015**, *137*, 10484-10487. DOI: 10.1021/jacs.5b06485
63. Tew, M. W.; Miller, J. T.; van Bokhoven, J. A., Particle Size Effect of Hydride Formation and Surface Hydrogen Adsorption of Nanosized Palladium Catalysts: L_3 Edge Vs K Edge X-Ray Absorption Spectroscopy. *J. Phys. Chem. C* **2009**, *113*, 15140-15147. DOI: 10.1021/jp902542f
64. Suleiman, M.; Jisrawi, N. M.; Dankert, O.; Reetz, M. T.; Bähtz, C.; Kirchheim, R.; Pundt, A., Phase Transition and Lattice Expansion During Hydrogen Loading of Nanometer Sized Palladium Clusters. *J. Alloys Compd.* **2003**, *356*, 644-648. DOI: 10.1016/S0925-8388(02)01286-0
65. Sitja, G.; Le Moal, S. V.; Marsault, M.; Hamm, G.; Leroy, F. D. R.; Henry, C. R., Transition from Molecule to Solid State: Reactivity of Supported Metal Clusters. *Nano Lett.* **2013**, *13*, 1977-1982. DOI: 10.1021/nl304741t
66. Duan, H.; Dong, J.; Gu, X.; Peng, Y.-K.; Chen, W.; Issariyakul, T.; Myers, W. K.; Li, M.-J.; Yi, N.; Kilpatrick, A. F. R., Hydrodeoxygenation of Water-Insoluble Bio-Oil to Alkanes Using a Highly Dispersed Pd–Mo Catalyst. *Nat. Commun.* **2017**, *8*, 1-10. DOI: 10.1038/s41467-017-00596-3
67. Wang, H.; Wang, H.; Kuhn, E.; Tucker, M. P.; Yang, B., Production of Jet Fuel-Range Hydrocarbons from Hydrodeoxygenation of Lignin over Super Lewis Acid Combined with Metal Catalysts. *ChemSusChem* **2018**, *11*, 285-291. DOI: 10.1002/cssc.201701567
68. Moos, G.; Emondts, M.; Bordet, A.; Leitner, W., Selective Hydrogenation and Hydrodeoxygenation of Aromatic Ketones to Cyclohexane Derivatives Using a Rh@SILP Catalyst. *Angew. Chem. Int. Ed.* **2020**, *59*, 11977-11983. DOI: 10.1002/anie.201916385
69. Lewis, F. A., The Hydrides of Palladium and Palladium Alloys. *Platin. Met. Rev.* **1960**, *4*, 132-137.
70. Ellis, I. T.; Wolf, E. H.; Jones, G.; Lo, B.; Li, M. M.-J.; York, A. P. E.; Tsang, S. C. E., Lithium and Boron as Interstitial Palladium Dopants for Catalytic Partial Hydrogenation of Acetylene. *Chem. Commun.* **2017**, *53*, 601-604. DOI: 10.1039/C6CC08404D
71. Zheng, Y.; Zhao, N.; Chen, J., Enhanced Direct Deoxygenation of Anisole to Benzene on SiO_2-Supported Ni-Ga Alloy and Intermetallic Compound. *Appl. Catal. B: Environ.* **2019**, *250*, 280-291. DOI: 10.1016/j.apcatb.2019.02.073
72. Kim, J. K.; Lee, J. K.; Kang, K. H.; Lee, J. W.; Song, I. K., Catalytic Decomposition of Phenethyl Phenyl Ether to Aromatics over Pd–Fe Bimetallic Catalysts Supported on Ordered Mesoporous Carbon. *J. Molec. Catal. A: Chem.* **2015**, *410*, 184-192. DOI: 10.1016/j.molcata.2015.09.023
73. Geng, D.; Zhu, S.; Chai, M.; Zhang, Z.; Fan, J.; Xu, Q.; Min, Y., Pd_XFe_Y Alloy Nanoparticles Decorated on Carbon Nanofibers with Improved Electrocatalytic Activity for Ethanol Electrooxidation in Alkaline Media. *New J. Chem.* **2020**, *44*, 5023-5032. DOI: 10.1039/C9NJ06086C

74. Feng, A.; Bai, J.; Shao, W.; Hong, W.; Tian, Z.-Q.; Xiao, Z., Surfactant-Free Pd–Fe Nanoparticles Supported on Reduced Graphene Oxide as Nanocatalyst for Formic Acid Oxidation. *Int. J. Hydrog. Energy* **2017**, *42*, 15196-15202. DOI: 10.1016/j.ijhydene.2017.04.278
75. Tang, Y.; Cao, S.; Chen, Y.; Lu, T.; Zhou, Y.; Lu, L.; Bao, J., Effect of Fe State on Electrocatalytic Activity of Pd–Fe/C Catalyst for Oxygen Reduction. *Appl. Surf. Sci.* **2010**, *256*, 4196-4200. DOI: 10.1016/j.apsusc.2010.01.124
76. Felicissimo, M. P.; Martyanov, O. N.; Risse, T.; Freund, H.-J., Characterization of a Pd–Fe Bimetallic Model Catalyst. *Surf. Sci.* **2007**, *601*, 2105-2116. DOI: 10.1016/j.susc.2007.02.023
77. Johnson, R. L.; Hanrahan, M. P.; Mellmer, M.; Dumesic, J. A.; Rossini, A. J.; Shanks, B. H., Solvent–Solid Interface of Acid Catalysts Studied by High Resolution MAS NMR. *J. Phys. Chem. C* **2017**, *121*, 17226-17234. DOI: 10.1021/acs.jpcc.7b04102
78. Pfennig, T.; Chemburkar, A.; Johnson, R. L.; Ryan, M. J.; Rossini, A. J.; Neurock, M.; Shanks, B. H., Modulating Reactivity and Selectivity of 2-Pyrone-Derived Bicyclic Lactones through Choice of Catalyst and Solvent. *ACS Catal.* **2018**, *8*, 2450-2463. DOI: 10.1021/acscatal.7b04311
79. Chang, B. S.; Martin, A.; Thomas, B.; Li, A.; Dorn, R. W.; Gong, J.; Rossini, A. J.; Thuo, M. M., Synthesis of Interface-Driven Tunable Bandgap Metal Oxides. *ACS Mater. Lett.* **2020**, *2*, 1211-1217. DOI: 10.1021/acsmaterialslett.0c00251
80. Brewer, C. E.; Schmidt-Rohr, K.; Satrio, J. A.; Brown, R. C., Characterization of Biochar from Fast Pyrolysis and Gasification Systems. *Environ. Prog. Sustain.* **2009**, *28*, 386-396. DOI: 10.1002/ep.10378
81. Huo, J.; Johnson, R. L.; Duan, P.; Pham, H. N.; Mendivelso-Perez, D.; Smith, E. A.; Datye, A. K.; Schmidt-Rohr, K.; Shanks, B. H., Stability of Pd Nanoparticles on Carbon-Coated Supports under Hydrothermal Conditions. *Catal. Sci. Technol.* **2018**, *8*, 1151-1160. DOI: 10.1039/C7CY02098H
82. de Souza, F. b. A.; Ambrozio, A. R.; Souza, E. S.; Cipriano, D. F.; Scopel, W. L.; Freitas, J. C., NMR Spectral Parameters in Graphene, Graphite, and Related Materials: Ab Initio Calculations and Experimental Results. *J. Phys. Chem. C* **2016**, *120*, 27707-27716. DOI: 10.1021/acs.jpcc.6b10042
83. Forse, A. C.; Griffin, J. M.; Presser, V.; Gogotsi, Y.; Grey, C. P., Ring Current Effects: Factors Affecting the NMR Chemical Shift of Molecules Adsorbed on Porous Carbons. *J. Phys. Chem. C* **2014**, *118*, 7508-7514. DOI: 10.1021/jp502387x
84. Harris, R. K.; Thompson, T. V.; Norman, P. R.; Pottage, C., Phosphorus-31 NMR Studies of Adsorption onto Activated Carbon. *Carbon* **1999**, *37*, 1425-1430. DOI: 10.1016/S0008-6223(99)00004-4
85. Xing, Y.-Z.; Luo, Z.-X.; Kleinhammes, A.; Wu, Y., Probing Carbon Micropore Size Distribution by Nucleus Independent Chemical Shift. *Carbon* **2014**, *77*, 1132-1139. DOI: 10.1016/j.carbon.2014.06.031
86. Kervern, G.; Pintacuda, G.; Zhang, Y.; Oldfield, E.; Roukoss, C.; Kuntz, E.; Herdtweck, E.; Basset, J.-M.; Cadars, S.; Lesage, A.; Copéret, C.; Emsley, L., Solid-State NMR of a Paramagnetic DIAD-Fe^{II} Catalyst: Sensitivity, Resolution Enhancement, and Structure-Based Assignments. *J. Amer. Chem. Soc.* **2006**, *128*, 13545-13552. DOI: 10.1021/ja063510n
87. Nayeem, A.; Yesinowski, J. P., Calculation of magic-angle spinning nuclear magnetic resonance spectra of paramagnetic solids. *J. Chem. Phy.* **1988**, *89*, 4600-4608. DOI: 10.1063/1.454800
88. Brough, A. R.; Grey, C. P.; Dobson, C. M., Paramagnetic ions as structural probes in solid-state NMR: distance measurements in crystalline lanthanide acetates. *J. Amer. Chem. Soc.* **1993**, *115*, 7318-7327. DOI: 10.1021/ja00069a034
89. Ro, I.; Aragao, I. B.; Brentzel, Z. J.; Liu, Y.; Rivera-Dones, K. R.; Ball, M. R.; Zanchet, D.; Huber, G. W.; Dumesic, J. A., Intrinsic Activity of Interfacial Sites for Pt-Fe and Pt-Mo Catalysts in the Hydrogenation of Carbonyl Groups. *Appl. Catal. B: Environ.* **2018**, *231*, 182-190. DOI: 10.1016/j.apcatb.2018.02.058
90. Haug, K. L.; Buergi, T.; Trautman, T. R.; Ceyer, S. T., Distinctive Reactivities of Surface-Bound H and Bulk H for the Catalytic Hydrogenation of Acetylene. *J. Amer. Chem. Soc.* **1998**, *120*, 8885-8886. DOI: 10.1021/ja9819615
91. Khan, N. A.; Shaikhutdinov, S.; Freund, H. J., Acetylene and Ethylene Hydrogenation on Alumina Supported Pd-Ag Model Catalysts. *Catal. Lett.* **2006**, *108*, 159-164. DOI: 10.1007/s10562-006-0041-y
92. Aramendıa, M. A.; Borau, V.; Jimenez, C.; Marinas, J. M.; Porras, A.; Urbano, F. J., Selective Liquid-Phase Hydrogenation of Citral over Supported Palladium. *J. Catal.* **1997**, *172*, 46-54. DOI: 10.1006/jcat.1997.1817
93. Bligaard, T.; Nørskov, J. K.; Dahl, S.; Matthiesen, J.; Christensen, C. H.; Sehested, J., The Brønsted–Evans–Polanyi Relation and the Volcano Curve in Heterogeneous Catalysis. *J. Catal.* **2004**, *224*, 206-217. DOI: 10.1016/j.jcat.2004.02.034

For Table of Contents Use Only

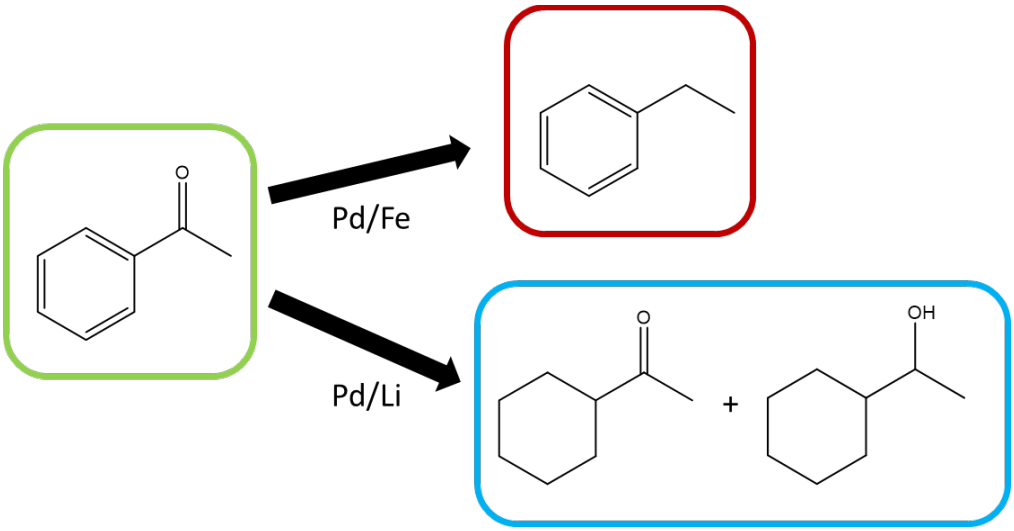

The hydrogenation/hydrodeoxygenation selectivity for a Pd on carbon-coated silica support catalys can be dramatically altered by selection of co-metal addition.